

## Photonic crystal heteroslab-edge microcavity with high quality factor surface mode for index sensing

Tsan-Wen Lu, Yi-Hua Hsiao, Wei-De Ho, and Po-Tsung Lee

Citation: *Applied Physics Letters* **94**, 141110 (2009); doi: 10.1063/1.3117225

View online: <http://dx.doi.org/10.1063/1.3117225>

View Table of Contents: <http://scitation.aip.org/content/aip/journal/apl/94/14?ver=pdfcov>

Published by the *AIP Publishing*

---

### Articles you may be interested in

[Photonic crystal slot nanobeam slow light waveguides for refractive index sensing](#)

*Appl. Phys. Lett.* **97**, 151105 (2010); 10.1063/1.3497296

[Silicon photonic crystal nanostructures for refractive index sensing](#)

*Appl. Phys. Lett.* **93**, 181103 (2008); 10.1063/1.3009203

[High quality factor microcavity lasers realized by circular photonic crystal with isotropic photonic band gap effect](#)

*Appl. Phys. Lett.* **90**, 151125 (2007); 10.1063/1.2724899

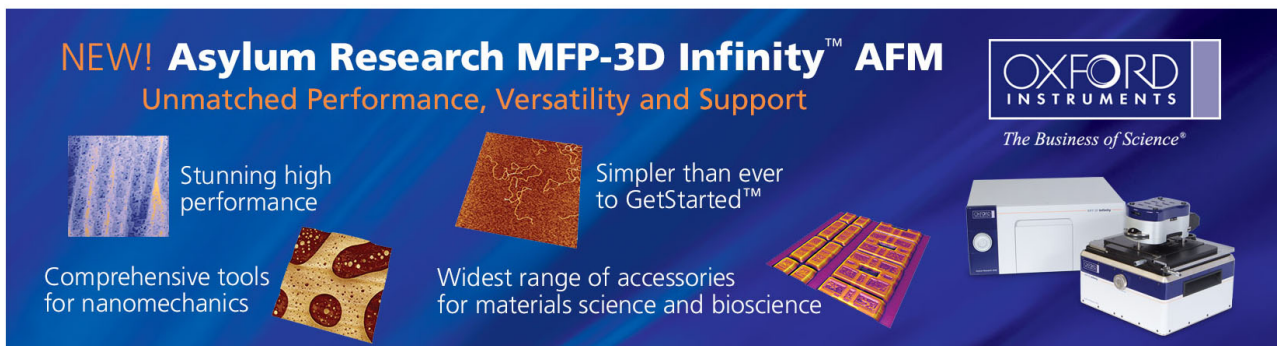
[High-quality-factor photonic crystal heterostructure laser](#)

*Appl. Phys. Lett.* **89**, 101104 (2006); 10.1063/1.2345912

[Experimental demonstration of a high quality factor photonic crystal microcavity](#)

*Appl. Phys. Lett.* **83**, 1915 (2003); 10.1063/1.1606866

---

The advertisement features a dark blue background with a subtle grid pattern. At the top left, the text 'NEW! Asylum Research MFP-3D Infinity™ AFM' is written in white and orange, followed by 'Unmatched Performance, Versatility and Support' in orange. The Oxford Instruments logo is in the top right. Below the main text are four images: a blue textured surface, a brown textured surface, a yellow textured surface, and a white AFM instrument. Each image is accompanied by a short text description. The AFM instrument is shown in a white and blue color scheme.

**NEW! Asylum Research MFP-3D Infinity™ AFM**  
Unmatched Performance, Versatility and Support

**OXFORD INSTRUMENTS**  
*The Business of Science®*

Stunning high performance  
Simpler than ever to GetStarted™

Comprehensive tools for nanomechanics  
Widest range of accessories for materials science and bioscience

# Photonic crystal heteroslab-edge microcavity with high quality factor surface mode for index sensing

Tsan-Wen Lu,<sup>a)</sup> Yi-Hua Hsiao, Wei-De Ho, and Po-Tsung Lee

Department of Photonics and Institute of Electro-Optical Engineering, National Chiao Tung University, Rm. 415, CPT Building, 1001 Ta-Hsueh Road, Hsinchu 300, Taiwan

(Received 17 February 2009; accepted 19 March 2009; published online 10 April 2009)

In this report, we propose a photonic crystal heteroslab-edge microcavity design for optical index sensing, where the high quality ( $Q$ ) surface mode is confined by mode-gap effect. By optimizing the barrier region of the microcavity, high  $Q$  factor of  $6.6 \times 10^5$  is obtained in simulations. Lasing actions with high  $Q$  factor and low threshold of 6400 and 0.55 mW are obtained from the real devices. High index sensing response and small detectable index variation of 625 nm per refractive index unit and  $3.6 \times 10^{-6}$  are obtained in simulations. © 2009 American Institute of Physics. [DOI: 10.1063/1.3117225]

For the past decades, the surface plasma wave<sup>1</sup> has been widely applied in demonstrating various optical sensors for chemical and biological applications, for example, gas compositions detecting, label-free biosensing, drug discovery, and so on. The surface plasma wave usually appears at the interface between metal with attenuation coefficient and dielectric material. Due to the field concentration at the surface of material, ultrahigh sensitivities in various designs have been proposed and demonstrated.<sup>2-4</sup> Generally, the surface plasma wave does not exist at the interface between dielectric materials. However, for photonic crystals (PhCs), due to the photonic band gap (PBG) effect, the surface wave can be sustained and propagate along the dielectric interfaces of two-dimensional (2D) and three-dimensional (3D) truncated PhCs.<sup>5,6</sup> Typically, in a 2D truncated PhC slab surrounded by air shown in Fig. 1(a), the surface wave is sustained in the slab edge both by PBG and total-internal reflection effects. In recent years, lots of interesting designs based on surface wave in 2D PhCs have been reported, including optical filters,<sup>7</sup> couplers,<sup>8</sup> waveguides with high transmissions and collimated emissions,<sup>9-11</sup> microcavities,<sup>12-14</sup> and so on, which are expected as important components in constructing versatile photonic integrated circuits (PhICs). Among above designs, the optical microcavities attract lots of attentions due to the abilities of well-confining photon flow locally in a condensed size and can be easily fused with other components by side-coupling ridge waveguides<sup>7</sup> in PhICs. By designing various PhC mirrors in truncated PhC slabs, microcavities with confined surface waves can be formed, which have been initiated demonstrated and discussed recently.<sup>12-14</sup>

One of the most attractive applications for optical microcavity is the optical index sensor. Very recently, high-sensitivity and condensed index sensors based on PhC defect micro- and nanocavities have been demonstrated and optimized theoretically,<sup>15,16</sup> which show the abilities of sensing very small index variation in very condensed size. In these reports, to increase the environmental index sensing response ( $R_n$ ), the defect mode fields are extended into environmental material (air) by modifying cavity geometries. High  $R_n$  val-

ues of 350 and 512 nm/RIU (refractive index unit) have been reported in experiments<sup>15</sup> and simulations,<sup>16</sup> respectively. To further increase  $R_n$ , intuitively, the PhC microcavity with confined surface wave would be a very good candidate because the mode field extends into environmental material, which has not been addressed and discussed in literatures. Besides, in addition to high  $R_n$  value, high quality ( $Q$ ) factor mode is also needed to provide fine optical spectral resolution and leads to high index sensitivity. Thus, in this report, we propose, fabricate, and characterize a PhC heteroslab-edge (HSE) microcavity design, where the surface mode is confined by mode-gap effect. The  $Q$  factor of surface mode is optimized in simulations by fine tuning the PhC barrier of the microcavity, which is aimed at achieving a high-sensitivity optical index sensor.

The scheme of a typical 2D truncated PhC slab surrounded by air is shown in Fig. 1(a). Different truncated terminations will lead to different surface mode profiles, which have been investigated in several reports.<sup>5,6,12</sup> The definition of the termination parameter  $\tau$  is also shown in Fig. 1(a). In the following designs,  $\tau$  is chosen as 0.25, where

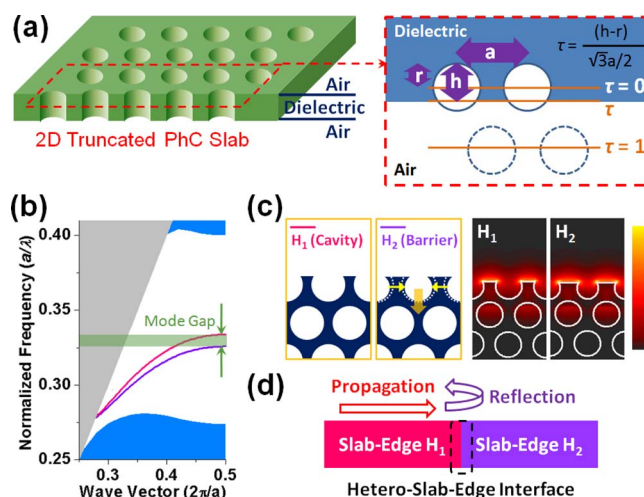


FIG. 1. (Color online) (a) Scheme of 2D truncated PhC slab surrounded by air and the definition of slab-edge termination parameter  $\tau$ . (b) The calculated dispersion curves, (c) unit cells, and mode profiles of surface modes propagating at PhC slab-edges  $H_1$  and  $H_2$ . (d) Scheme of HSE interface formed by different slab-edges  $H_1$  and  $H_2$ .

<sup>a)</sup>Electronic mail: ricky.eo94g@nctu.edu.tw. Tel.: 886-3-5712121 ext. 59345. FAX: 886-3-5735601.

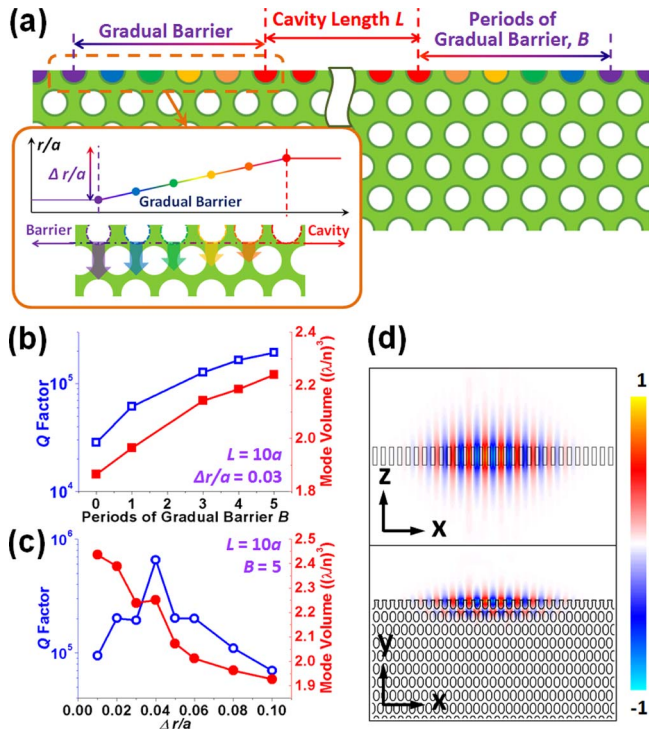


FIG. 2. (Color online) (a) Scheme of PhC HSE microcavity. The gradual PhC barrier is formed by gradually shrinking air holes at the slab edge. The simulated  $Q$  factor and  $V$  versus parameters (b)  $B$  and (c)  $\Delta r/a$ . (d) The simulated surface mode profiles in electrical field in  $x$ - $z$  (top) and  $x$ - $y$  (bottom) planes when  $L = 10a$ ,  $B = 5$ , and  $\Delta r/a = 0.04$ .

the surface mode frequency lies near the midgap of PBG region. The dispersion curve of this surface mode obtained by plane-wave-expansion method is shown as the peach curve in Fig. 1(b). The unit cell (denoted as  $H_1$ ) and the simulated surface mode with energy concentrations in the air are shown in Fig. 1(c). To confine the surface mode at the slab edge locally, we design a barrier region by shrinking and shifting the air holes at the slab edge, which is shown and denoted as  $H_2$  in Fig. 1(c). When the air holes are modified as described above, the surface mode frequency will become lower as shown by the purple curve in Fig. 1(b). For a 2D truncated PhC HSE interface formed by slab-edges  $H_1$  and  $H_2$  shown in Fig. 1(d), the surface mode with frequency inside the range indicated by green shadow region in Fig. 1(b) will propagate in slab-edge  $H_1$  and regards the slab-edge  $H_2$  as a mirror, which forms the well-known mode-gap effect.<sup>17,18</sup> Thus, we can design a microcavity by applying double HSE interfaces as shown in Fig. 2(a), which is named PhC HSE microcavity.

In our PhC HSE microcavity design, the air-hole radius ( $r$ ) over lattice constant ( $a$ ) ( $r/a$ ) ratios of PhC lattice [white circles in Fig. 2(a)] and microcavity region (red circles) are the same (fixed  $r$  and  $a$ ) and set to be 0.36 initially. The microcavity length  $L$ ,  $\tau$ , and slab thickness are set to be  $10a$ ,  $0.25$ , and  $220$  nm, respectively. The barrier region with mode-gap effect is designed by shrinking and shifting the air holes at the slab edge, as illustrated in Fig. 1(c). To obtain high  $Q$  microcavity, the air holes of the barrier region are shrunk and shifted gradually, from orange to purple circles shown in Fig. 2(a). The number of periods of the gradual barrier region is denoted as  $B$ . This gradual barrier design is mainly expected for gentle mode-gap confinement<sup>17,18</sup> and the reduction of optical scattering losses in the barrier region.

The  $r/a$  ratios of the remaining outer barrier region with purple circles in Fig. 2(a) are kept the same, and the  $r/a$  ratio difference between microcavity and outer barrier is denoted as  $\Delta r/a$ . Thus, the  $r/a$  difference between air holes in the gradual barrier region is  $\Delta r/a \times 1/B$ .

To optimize the  $Q$  factor of PhC HSE microcavity, we vary the parameter  $B$  from 0 to 5 with  $\Delta r/a = 0.03$ . The simulated  $Q$  factor and effective mode volume  $V$  by a 3D finite-difference time-domain (FDTD) simulations are shown in Fig. 2(b). When  $B = 0$  (no gradual barrier), the low  $Q$  factor of  $2.8 \times 10^4$  is mainly attributed to the scattering losses of the HSE interface with sharp  $r/a$  ratio variation between barrier and microcavity. Once the gradual barrier periods increase, the gentle confinement due to gentle  $r/a$  ratio variation will be provided, which leads to the increased  $Q$  factor. When  $B = 5$ , the  $Q$  factor increases to  $2 \times 10^5$ . Besides, the mode volume also increases monotonically with  $B$ . This indicates the mode profile extends more into the gradual barrier region, which is caused by the gentler mode confinement.<sup>17</sup>

Then we further optimize the  $Q$  factor by varying  $\Delta r/a$  from 0.01 to 0.1 when  $B = 5$ . The simulated results are shown in Fig. 2(c). When  $\Delta r/a$  is small, the mode-gap confinement is weak and the mode will extend into the barrier, which leads to low  $Q$  factor and large mode volume. On the other hand, when  $\Delta r/a$  becomes too large, extra scattering losses are induced due to sharp mode confinement. Therefore, the  $Q$  factor is decreased and less mode profile extends into the gradual barrier region, which leads to small mode volume. Thus, we obtain an optimized high  $Q$  factor of  $6.6 \times 10^5$  when  $\Delta r/a = 0.04$  with  $V$  of  $2.25 \times (\lambda/n)^3$ . The simulated surface mode profiles in electrical field in  $x$ - $z$  and  $x$ - $y$  planes are shown in Fig. 2(d). From Fig. 2(d), one can observe the significant electrical field concentrations in the air region, which implies high sensitivity of this surface mode to the environmental index variation.

In fabrication, the real devices are fabricated on an epitaxial structure consisting of four 10 nm InGaAsP quantum wells by electron-beam lithography and a series of reactive ion etching and inductively coupled plasma etching process. Then the membrane structure is formed by HCl selective wet-etching process. The scanning electron microscope (SEM) pictures of fabricated PhC HSE microcavity are shown in Figs. 3(a)–3(d). The fabricated  $\tau$ ,  $a$ ,  $r/a$ ,  $\Delta r/a$ ,  $L$ , and  $B$  are 0.24, 510 nm, 0.38, 0.08,  $10a$ , and 5, respectively. The  $\Delta r/a$  is a little enlarged due to proximity effect from electron-beam lithography, which can be further optimized.

The devices are optically pumped by a pulsed diode laser with 0.5% duty cycle at room temperature. The typical light-in light-out ( $L$ - $L$ ) curve is shown in Fig. 4(a) and the threshold is estimated to be 0.55 mW at pump position A. The lasing spectrum near 1550 nm is shown in Fig. 4(b) by curve A. The measured spectral linewidth near threshold is estimated to be 0.24 nm by Lorentzian fitting, which is shown in the inset of Fig. 4(a) and corresponds to a  $Q$  factor of 6400. To further confirm light localization at the HSE microcavity, the pump position is moved outside the microcavity to positions B, C, and D, respectively, and no lasing action is observed, as shown in Fig. 4(b). Besides, the measured polarization with polarized ratio of 8 shown in the inset of Fig. 4(b) also indicates the surface mode resonance along the slab edge.



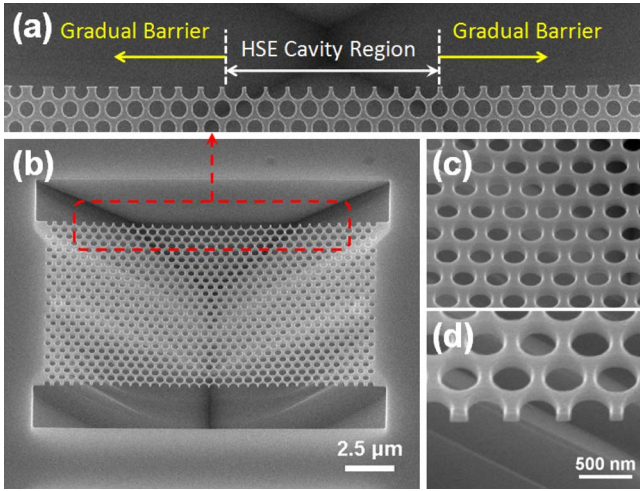


FIG. 3. (Color online) SEM pictures of fabricated PhC HSE microcavity, including (a) top-view, (b) tilted-view of fabricated device, and zoom-in tilted-view of fabricated (c) PhC and (d) slab edge.

To address the potential of our PhC HSE microcavity serving as a high-sensitivity index sensor, we calculate the  $R_n$  value by setting the environmental index from 1 (air) to 1.02 (with gases) in 3D FDTD simulations. The optimized HSE microcavity design with  $Q$  factor of  $6.6 \times 10^5$  in Fig. 2(c) is applied. The calculated wavelength variation of 12.5 nm when the environmental index varied from 1 to 1.02 is shown in Fig. 4(c), which corresponds to a large  $R_n$  value of 625 nm/RIU. This is mainly attributed to the characteristic of

surface mode field extending into the environmental air region, which leads to high sensitivity to environmental index variation. The detectable index variation  $\Delta n_{\text{det}}$  can be obtained by inserting  $R_n$  and  $Q$  into following expression:

$$\Delta n_{\text{det}} = \frac{1}{R_n} \times \frac{\lambda}{Q},$$

where  $\lambda$  and  $\lambda/Q$  denote the wavelength and optical spectral linewidth, respectively. The calculated  $\Delta n_{\text{det}}$  is as small as  $3.6 \times 10^{-6}$ . This small value actually can be further decreased by optimizing the parameter  $\tau$  and  $r/a$  ratio of PhC HSE microcavity for higher  $R_n$  value and  $Q$  factor. We believe the very small  $\Delta n_{\text{det}}$  close to that of conventional interferometer can be expected and achieved by this PhC microcavity design, which is with very condensed device size.

In summary, we propose a PhC HSE microcavity design for serving as an optical index sensor, where the high  $Q$  surface mode is confined by mode-gap effect provided by the gradual barrier design. By optimizing the parameters  $B$  and  $\Delta r/a$  of the gradual barrier region in 3D FDTD simulations, we obtain high  $Q$  factor of  $6.6 \times 10^5$  from the confined surface mode. In experiments, the surface mode lasing action with high  $Q$  factor and low threshold of 6400 and 0.55 mW is obtained from the real devices. Besides, based on this HSE microcavity design, high index sensing response  $R_n$  and small detectable index variation  $\Delta n_{\text{det}}$  of 625 nm/RIU and  $3.6 \times 10^{-6}$  are obtained in simulations. Both values indicate the great potential of PhC HSE microcavity serving as a high-sensitivity optical index sensor with very condensed device size.

This work is supported by Taiwan's National Science Council (NSC) under Contract Nos. NSC-95-2221-E-009-056-MY3 and NSC-97-2120-M-009-004. The authors would like to thank the help from Center of Nano Science and Technology (CNST) of National Chiao Tung University (NCTU), Taiwan.

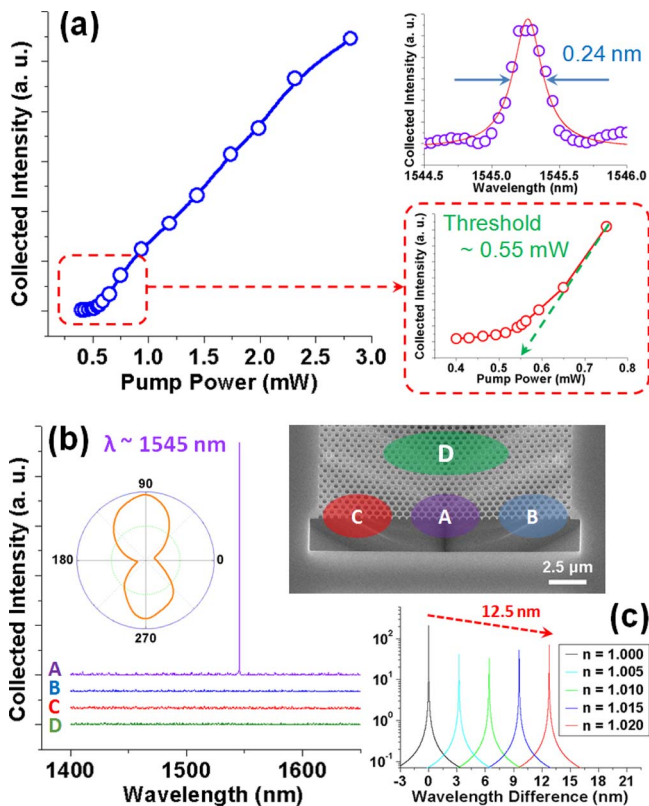


FIG. 4. (Color online) (a)  $L$ - $L$  curves and spectrum near threshold with Lorentzian fitting. (b) Lasing spectrum (curve A) near 1550 nm when pumping the cavity region (position A) and spectra (curves B, C, and D) when pumping outside the cavity region (positions B, C, and D). The measured polarization with polarized ratio of 8 is also shown. (c) The simulated surface mode wavelength variation of 12.5 nm when the environmental index is varied from 1 to 1.02.

<sup>1</sup>R. H. Ritchie, *Phys. Rev.* **106**, 874 (1957).

<sup>2</sup>A. Lesuffleur, H. S. Im, N. C. Lindquist, and S. H. Oh, *Appl. Phys. Lett.* **90**, 243110 (2007).

<sup>3</sup>R. Micheletto, K. Hamamoto, T. Fujii, and Y. Kawakami, *Appl. Phys. Lett.* **93**, 174104 (2008).

<sup>4</sup>C. J. Alleyne, A. G. Kirk, R. C. McPhedran, N. P. Nicorovici, and D. Maystre, *Opt. Express* **15**, 8163 (2007).

<sup>5</sup>R. D. Meade, K. D. Brommer, A. M. Rappe, and J. D. Joannopoulos, *Phys. Rev. B* **44**, 10961 (1991).

<sup>6</sup>W. M. Robertson, G. Arjavalingam, R. D. Meade, K. D. Brommer, A. M. Rappe, and J. D. Joannopoulos, *Opt. Lett.* **18**, 528 (1993).

<sup>7</sup>Z. Zhang, M. Dainese, L. Wosinski, S. Xiao, M. Qiu, M. Swillo, and U. Andersson, *Appl. Phys. Lett.* **90**, 041108 (2007).

<sup>8</sup>H. C. Chen, K. K. Tsia, and A. W. Poon, *Opt. Express* **14**, 7368 (2006).

<sup>9</sup>E. Moreno, F. J. Garcia-Vidal, and L. Martin-Moreno, *Phys. Rev. B* **69**, 121402 (2004).

<sup>10</sup>W. Smigaj, *Phys. Rev. B* **75**, 205430 (2007).

<sup>11</sup>E. H. Khoo, T. H. Cheng, A. Q. Liu, J. Li, and D. Pinjala, *Appl. Phys. Lett.* **91**, 171109 (2007).

<sup>12</sup>J. K. Yang, S. H. Kim, G. H. Kim, H. G. Park, Y. H. Lee, and S. B. Kim, *Appl. Phys. Lett.* **84**, 3016 (2004).

<sup>13</sup>S. Xiao and M. Qiu, *Appl. Phys. Lett.* **87**, 111102 (2005).

<sup>14</sup>S. Xiao and M. Qiu, *J. Opt. Soc. Am. B* **24**, 1225 (2007).

<sup>15</sup>S. Kita, K. Nozaki, and T. Baba, *Opt. Express* **16**, 8174 (2008).

<sup>16</sup>S. H. Kwon, T. Sunner, M. Kamp, and A. Forchel, *Opt. Express* **16**, 11709 (2008).

<sup>17</sup>B. S. Song, S. Noda, T. Asano, and Y. Akahane, *Nature Mater.* **4**, 207 (2005).

<sup>18</sup>S. H. Kwon, T. Sunner, M. Kamp, and A. Forchel, *Opt. Express* **16**, 4605 (2008).